ELSEVIER

Chemical Engineering Journal 121 (2006) 1–8

Chemical Engineering Journal

www.elsevier.com/locate/cej

Modelling prediction of the microcapsule size of polyelectrolyte complexes produced by atomization

Edgar P. Herrero, E.M. Martín Del Valle *, M.A. Galán

Department of Chemical Engineering, University of Salamanca, P/Los Caídos S/N, 37008 Salamanca, Spain

Received 30 November 2005; received in revised form 17 April 2006; accepted 19 April 2006

Abstract

In order to have a better understanding of the atomization process for microencapsulation applications the disintegration of polymer liquid jets (sodium alginate) injected into high-velocity gas streams was studied and a mathematical model to predict the microparticle size has been developed.

Air-blast atomization of viscous non-Newtonian fluid (alginate solution) was carried out in order to produce microbeads (1–50 μm) based on polyelectrolyte complexes with particle size control and a particle size distribution with a relative span factor, $(D_{0.9} - D_{0.1})/D_{0.5}$, less than 1.4. The accuracy of the wave-mechanisms-based models in predicting droplet size after breakup of alginate solution has been demonstrated. The atomized microparticle size were expressed in terms of three dimensionless groups, the liquid/air mass ratio, the Weber number and the Ohnesorge number in simple forms whose exponents and coefficients were determined by least-squares fit to the experimental data. With these data two semi-empirical models have been proposed to predict the particle size obtained from the microencapsulation. Both models allow the prediction of particle size of the microcapsules obtained by atomization processes.

Keywords: Air-blast atomization; Particle size prediction; Wave mechanisms

1. Introduction

In the rapidly changing scientific world, contributions of scientists and engineers are leading to major new solutions of significant medical problems [1,2].

The most common method of administration of drugs is in the form of pills or injections. These methods of administration meet the requirements of efficacy for several drugs, with regard to the introduction and elimination of the drug in the organism, its absorption in blood, and its distribution to points where it is necessary. However, these methods are inadequate for many new drugs such as hormones and vaccines. These protein drugs are usually high molecular weight proteins and are very sensitive to environmental conditions. Most proteins cannot be delivered orally due to problems related to degradation in the acidic environment of the gastrointestinal tract. Moreover, the high molecular weight of these substances often results in poor absorption in to the blood stream when administered orally. The most common mode of administration of these therapeutic proteins is intravenous injections, which are usually not well tolerated by the recipient. Also, most of these proteins have short half-lives in the blood stream and need to be administered frequently in high doses to obtain therapeutic efficacy. Systemic administration in high doses can lead to side effects and can also be toxic. To overcome these difficulties, new technologies, like the microencapsulation, have been developed [3–6]. Microencapsulation is a process by which the active material is enclosed in a polymeric matrix and surrounded by a coating to produce capsules in the micrometer range known as microcapsules. The most important application of this technology is the immobilization of stem cells for cellular therapy to the treatment of the most devastating diseases. To do that, is needed the administration of the microcapsules via injection Hamilton and aerosol that requires particles diameter below 50 μm.

These technologies are based on the use of polymers. Polysaccharides, such as alginate, have been widely used in the microencapsulation technology. Alginate is a water-soluble linear polysaccharide extracted from brown seaweed, and is composed of alternating blocks of 1-4-linked α-L-guluronic and β-D-mannuronic acid residues. Alginate has an excellent bio-

* Corresponding author.
E-mail address: emvalle@usal.es (E.M.M. Del Valle).

1385-8947/$ – see front matter © 2006 Elsevier B.V. All rights reserved.
doi:10.1016/j.cej.2006.04.003

Nomenclature

A	Amplitude of surface waves (m)
C_{Do}	Drag coefficient of a cylinder in cross-flow
d_i	Diameter of droplet (μm)
D	Injector exit diameter, diameter of liquid jet (μm)
$D_{0.1}$	Diameter at the 10th percentile (μm)
$D_{0.5}$	Diameter at the 50th percentile (μm)
$D_{0.9}$	Diameter at the 90th percentile (μm)
$\dot{M}_a$	Air mass flow rate (g/s)
$\dot{M}_l$	Liquid mass flow rate (g/s)
n^*	Shock dynamic pressure ratio
N_i	number of droplets
SMD	Sauter mean diameter (μm)
t	Time (s)
u	Wave velocity (m/s)
U_a	Gas phase average velocity (m/s)
U_l	Velocities of the liquid (m/s)
V_d	Velocity of the atomized drop and the atomizing air after transferring part of its kinetic energy to the liquid (m/s)
We	Weber number = $(We = \rho_a U_a^2 D/\sigma)$
X_{We}	Power dependence of SMD on Weber number
X_Z	Power dependence of SMD on viscosity or Ohnesorge number
X_1	General correlation exponents
$X_{2,3}$	General correlation coefficients
Z	Ohnesorge number = $(We)^{1/2}/Re = \mu_l/(\rho_l \sigma D)^{1/2}$

Greek letters

β	Jeffrey's sheltering parameter
ζ	Angle between the jet axis and gas velocity (radian)
λ	Wavelength of a disturbance (m^{-1})
μ	Newtonian viscosity (Ns/m^2)
ν	Kinematic viscosity (m/s^2)
ρ_a	Air density (kg/m^3)
ρ_l	Liquid density ($kg/m^{3)}$
σ	Surface tension (N/m)

Superscript

(-)	Mean velocity or density evaluated before of the break-up of the liquid jet

compatibility and biodegradability. Alginates have the ability to form gels by reaction with divalent cations such as calcium or barium. The aqueous solutions of alginates have shear-thinning characteristics, i.e. the viscosity decreases with increasing shear rate (stirrer speed). This property is also called pseudoplasticity, or non-Newtonian fluid. The viscosity of an alginate solution depends on the concentration of alginate and the length of the alginate molecules, i.e. the number of monomer units in the chains. The longer the chains the higher the viscosity at similar concentrations [7].

Most methods of microencapsulation involve one of two harsh conditions (contact with an organic solvent and/or heating during processing), which usually is a problem, especially for biomaterials handling [4,5]. The previous work done on microencapsulation without harsh conditions produce capsules with diameters ranged between 300 and 1000 μm [6–14].

Several attempts have been done in order to produce very small particles based on polyelectrolyte complexes, but there is not a technology able to produce these microcapsules below 300 μm, with control size and a particle size distribution with a relative span factor less than 1.4 [8–14].

For that reason, based in atomization processes, a microencapsulation technology of polyelectrolyte complex beads (alginate–barium), which produced very small particles (1–50 μm) has been developed.

Atomization is a process in which the disruptive action of externally applied aerodynamic forces is opposed by the consolidating influences of the liquid viscosity and surface tension forces. Disintegration of liquid jets injected into quiescent and high-velocity gas streams has been studied by many researchers. Theoretical and experimental studies on the mechanism of atomization have been carried out by Rayleigh, Tyler, Weber, Haenlein, Ohnesorge and Castleman [15]. Detailed reviews of earlier work have been published by Giffen and Muraszew [16], and more recently by Chigier [17], and Lefebvre [15].

During the last decade atomization techniques as air-blast or twin-fluid atomization has been widely used taking the place of spray drying [12–14].

In air-blast atomization, low-speed liquid jets are accelerated by the surrounding high-speed gas flow, usually in the spray flow direction. The liquid is subjected to both tensile and shearing stresses. The magnitude of the extension has been shown to be significant for applications involving polymer solutions. Twin-fluid atomizers have a number of advantages over pressure atomizers including lower requirements for the liquid injection pressure and finer sprays. Unfortunately, the process of air-blast atomization is very complex and its physical mechanisms are not fully understood [15].

Therefore, in order to have a better understanding of the atomization process for microencapsulation applications the disintegration of polymer liquid jets (sodium alginate) injected into high-velocity gas streams were studied. Two semi-empirical models of air-blast atomization based on the wave mechanism of breakup of non-Newtonian polymer have been developed. Both models allow the prediction of particle size of the microcapsules obtained by atomization processes. The experimental data of the microcapsules size were compared with the models predictions.

2. Materials and methods

2.1. Material

Sodium alginate from macrocystis pyrifera (medium viscosity) was purchased from Sigma Chemicals, barium chloride dihydrate, reagent grade was purchased from Scharlau.

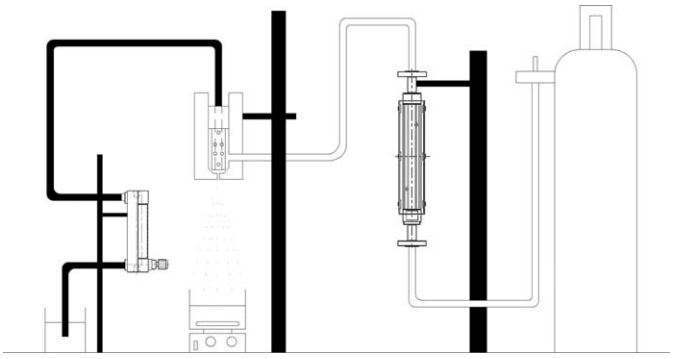

Fig. 1. A scheme of the microencapsulation device. 1, sodium alginate solution (0.7 wt.%); 2, rotameter of sodium alginate; 3, nozzle; 4, hardening solution ($BaCl_2$) (2 wt.%); 5, rotameter of air; 6, pressurized air.

2.2. Production of microcapsules

The generation of the microcapsules, optimized to produce microcapsules in the size range of 1–50 μm, can be described as follows. Sodium alginate (0.7 wt.%) was fed from a beaker to an atomization nozzle of 1.8 mm by air intake. After that, sodium alginate is sprayed into a crystallizer containing 1000 ml of hardening solution, 2 wt.% barium chloride solution, which induces the gelation. The device to the atomization works with pressurized air that mixes with the liquid, forcing liquid droplets out through the orifice of the nozzle. The divalent barium ions cross-link the droplets of sodium alginate on contact to form the microcapsules. The microbeads were kept 5 min under cross-linked conditions to form a semi-permeable membrane. The resultant microbeads were collected by filtration and washed with 30 ml of 0.9% of barium chloride and kept in distilled water. The scheme of the microencapsulation device is shown in Fig. 1.

The experimental conditions span a wide range of Weber numbers and are presented in Table 1.

2.3. Particle size analysis

We have obtained the particle size distribution of the microcapsules produced with laser diffractometry. To do that we have used a Leeds and Northrup Microtac Particle Size Analyzer. This device utilizes the phenomenon of scattered light from a laser beam projected through a stream of particles.

The droplet size distribution is frequently characterized by its Sauter mean diameter (SMD), which is the diameter of that drop whose volume/surface ratio value is the same as the arithmetic mean of volume/surface values on the total number of drops belonging to the sample spray under examination. Usually the concept of SMD is defined as:

$$\mathrm{SMD} = \frac{\int_0^\infty D^3 \,\mathrm{d}N}{\int_0^\infty D^2 \,\mathrm{d}N} \tag{1}$$

where, D is the droplet diameter, and dN stands for the percentage of the total number of droplets with a diameter contained in the interval $[D, D + \mathrm{d}D]$.

The SMD is influenced by the properties of the atomized and atomizing fluids and by the nozzle design and operating conditions.

Table 1
Experimental conditions

Alginate flow rate (g/s)	3.00–37.00
Alginate exit velocity (m/s)	0.02–0.24
Air mass flow rate (g/s)	101.17–178.00
Air exit velocity (m/s)	513.49–903.84
Weber number, *We*	9492.10–29409.55
Alginate kinematic viscosity (m^2/s)	6.45×10^{-5}
Surface tension (N/m)	0.054
Ohnesorge number, *Z*	0.21

3. Wave mechanisms and size distribution

In various ways of atomization, small disturbances in the jet or sheet will start growing across the liquid, which eventually disintegrates into ligaments and then drops, thus increasing the specific surface area of the liquid exposed to the gas medium and thereby achieving high rates of heat transfer, mixing and evaporation.

Essentially, all that is needed for liquid atomization is a high relative velocity between the liquid to be atomized and its surrounding air or gas. This can be achieved through the increase of the liquid kinetic energy, or by the exposure of relative slow moving liquid to a high air or gas velocity, or by applying external mechanical energy on the liquid through the utilization of a rotating or vibrating device to increase the energy carried within the liquid to over come the consolidating surface tension force. Based on the forms of energy applied, atomizers are classified into pressure atomizer, pressure swirl atomizer, twin-fluid atomizer, rotary atomizers, electrostatic and ultrasonic atomizers, etc. [15]

In this work a twin-phased gas–liquid atomizer was used. In this way, the kinetic energy carried with high velocity gas stream is utilized to disintegrate the relatively low velocity liquid sheet or jet into droplets. A variety of these atomizers is the air-blast atomizer, in which, an annular liquid sheet exiting from the atomizer is exposed to an inner and an outer air streams moving at high velocities (Fig. 2). The liquid is subjected to both tensile and shearing stresses.

The wave mechanism has found the widest acceptance among the mechanisms of atomization. In this theory the disintegration of liquid sheets or liquid jets is caused by the growth of unstable waves at the liquid–gas interface due to the aerodynamic interactions between the liquid and the gas. This type of instability is referred to as Kelvin-Helmholtz instability [18] and is characterized by unstable waves that appear in the fluid interface between two superimposed fluids of differing densities and velocities.

A number of previous studies [20,21] indicate that the curvature effect may be negligible due to the relatively small thickness of the liquid sheet compared to the radius of curvature. As a result, the liquid to be atomized may be modelled in a first approximation as a plane liquid sheet [22].

The waves are generated by factors such as pressure fluctuations or turbulence in the gas stream or liquid stream [23,24].

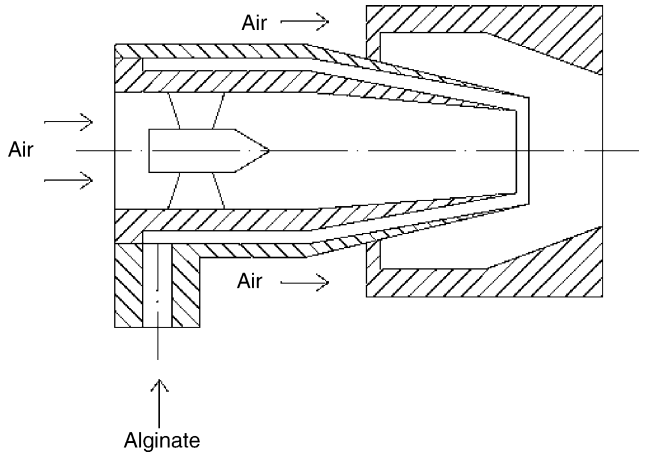

Fig. 2. Schema of a pre-filming air-blast atomizer.

Due to aerodynamic interactions, the perturbations grow in magnitude and reach a maximum value. When the dynamic pressure ($\rho_a U_a^2/2$) of the air stream in air-blast atomization is large enough, the amplitude of the surface waves will grow if their wavelength (λ) exceeds a minimum value [23–26]. There exists a dominant or most unstable wave number corresponding to the maximum growth rate and when the amplitude of the disturbance reaches a critical value, the wave detaches from the sheet to form shreds or ligaments, which rapidly collapse, forming drops. This process is shown in Fig. 3.

The system of forces acting on the slightly disturbed surface of a liquid sheet moving in air, are shown in Fig. 4. Surface tension forces try to return the protuberance back to its original position, but the air experiences a local decrease in static pressure (corresponding to the local increase in velocity) that tends to expand the protuberance farther outward. This corresponds to the normal pattern of wind-induced instability, where surface tension forces oppose any movement of the interface from its initial plane and attempt to restore equilibrium, while the aerodynamic forces increase any deviation from the interface and thereby promote instability.

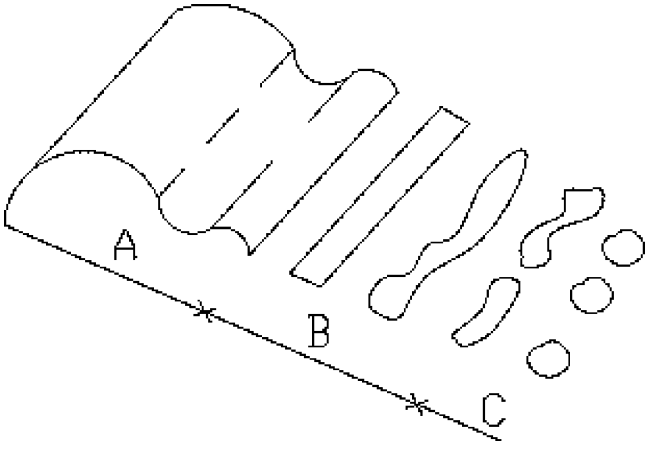

Fig. 3. Disintegration of the liquid sheet [19]. (A) Growth of unstable waves, (B) formation of ligaments, (C) breakup of ligaments into droplets.

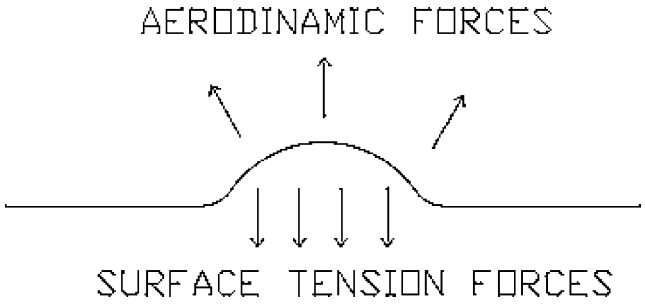

Fig. 4. System of forces acting on a liquid sheet moving in air.

The amplitude (A) of the surface waves on the liquid is described by the following differential equation [25]:

$$\frac{dA}{dt} = A\left[\frac{\pi\beta\rho_a(U_a-u)^2}{\lambda\rho_l u} - \frac{8\pi^2\mu_l}{\rho_l\lambda^2}\right] \tag{2}$$

where the subscript 'l' refers to liquid phase properties and the subscript 'a' refers to gas phase properties. From Eq. (2), it is seen that the amplitude, damped by liquid viscous force, increase as the air velocity increase. When both the aerodynamic pressure force and the surface tension forces are significant, the wave velocity u is given by [23]:

$$u = \left[\frac{a\lambda}{2\pi} + \frac{2\pi\sigma}{\lambda\rho_l}\right]^{1/2} \tag{3}$$

where a is the acceleration caused by the aerodynamic drag on the liquid jet, described by:

$$a = \frac{4C_{Do}\sin^2\zeta}{\pi D\rho_l}\left(\frac{\bar{\rho}_a\bar{U}_a^2}{2}\right) \tag{4}$$

where C_{Do} is the drag coefficient, ζ is the angle between the air and the liquid stream, D is the diameter of the liquid jet, and $\bar{\rho}_a\bar{U}_a^2/2$ is the free stream aerodynamic pressure. Substituting Eq. (3) into Eq. (2) and assuming $U_a \gg u$ leads to the following equation:

$$\frac{dA}{dt} = A\left[\frac{\pi\beta\rho_a U_a^2}{\lambda\rho_l[(a\lambda/2\pi)+(2\pi\sigma/\lambda\rho_l)]^{1/2}} - \frac{8\pi^2\mu_l}{\rho_l\lambda^2}\right] \tag{5}$$

Eq. (5) shows that the amplitude growth is resisted by surface tension (σ). Note that in this study the liquid velocity is negligibly small compared to the air velocity.

The minimum wavelength λ_m, above which the amplitude grows exponentially with time, may be estimated by setting $dA/dt = 0$. This results in the following cubic expression for λ_m:

$$\lambda_m^2 - \lambda_a\lambda_m^2 - \lambda_\sigma^2 = 0 \tag{6}$$

where

$$\frac{\lambda_\sigma}{D} = \frac{2\pi(16)^{1/3}}{\beta^{2/3}}\left(\frac{Z}{We}\right)^{2/3} \tag{7}$$

$$\frac{\lambda_a}{D} = \frac{64C_{Do}\sin^2\zeta}{n^*\beta^2\pi}\left(\frac{Z^2}{We}\right) \tag{8}$$

where λ_σ and λ_a are the wavelengths of the capillary waves and acceleration waves, respectively, and $n^* = \rho_a U_a^2/\bar{\rho}_a\bar{U}_a^2$

the shock dynamic pressure ratio. The Weber number ($We = \rho_a U_a^2 D/\sigma$) represents the ratio of aerodynamic force to surface tension. And the Ohnesorge number ($Z = \mu_l/(\rho_l \sigma D)^{1/2}$) contains only the properties of the globules formed in primary atomization before they split up into smaller drops during secondary atomization. It is sometimes called a stability group because it provides an indication of the resistance of a globule to further disintegration, but it is also called a viscosity group because it accounts for the effect of liquid viscosity on the globule.

When the aerodynamic pressure force predominates, waves propagate as acceleration waves at a minimum velocity of $(a\lambda_m/2\pi)^{1/2}$. In this case, $\lambda_a \ll \lambda_\sigma$, and one solution to Eq. (6) is $\lambda_a = \lambda_\sigma$, which is governed by $(Z/We)^{2/3}$, as shown in Eq. (7). In contrast, when the surface tension predominates, waves propagate as capillary waves at a minimum velocity of $(2\pi\sigma/\lambda_m\sigma_l)^{1/2}$. Since $\lambda_\sigma \ll \lambda_a$, one solution to Eq. (6) is $\lambda_m = \lambda_a$, which is governed by Z^2/We, as shown in Eq. (8).

Additionally, the dimensionless ratio liquid/air should be considered in atomization processes. Rizt and Lefebvre [27] showed that the liquid/air interaction produces waves that become unstable and disintegrate into fragments. These fragments then contract into ligaments, which in turn break down into drops. They proved that with increase in air velocity, the liquid sheet disintegrates earlier and ligaments are formed nearer the lip. These ligaments tend to be thinner and shorter and disintegrate into smaller drops. Arai and Hashimoto [28] for a constant liquid sheet thickness, showed that breakup length decrease with increase in the relative velocity between the air and the liquid. Also, they prove that breakup length increases as the liquid sheet velocity increases or as the liquid viscosity decrease.

3.1. Dependence of SMD on fluid viscosity or the Ohnesorge number

Mansour and Chigier [29] studied the influence of the fluid viscosity on the Sauter mean diameter for non-Newtonian fluids. They found that the SMD increase with the apparent viscosity of the fluid according to the equation:

$$\text{SMD} = f(Z^{X_Z}) \tag{9}$$

The value of X_Z was found insensitive to the variations in the air mass flow rate or air velocity.

3.2. Dependence of SMD on $(1 + (\dot{M}_l/\dot{M}_a))$

The power dependence on $(1 + (\dot{M}_l/\dot{M}_a))$ is examinated by plotting the SMD data as a function of $(1 + (\dot{M}_l/\dot{M}_a))$ at constant Weber number. Using a logarithmic plot (Fig. 5) of these data the following equation was found:

$$\text{SMD} = f\left(1 + \frac{\dot{M}_l}{\dot{M}_a}\right)^{2.66} \tag{10}$$

where $\dot{M}_l$ and $\dot{M}_a$ are the liquid mass flow and the air mass flow, respectively.

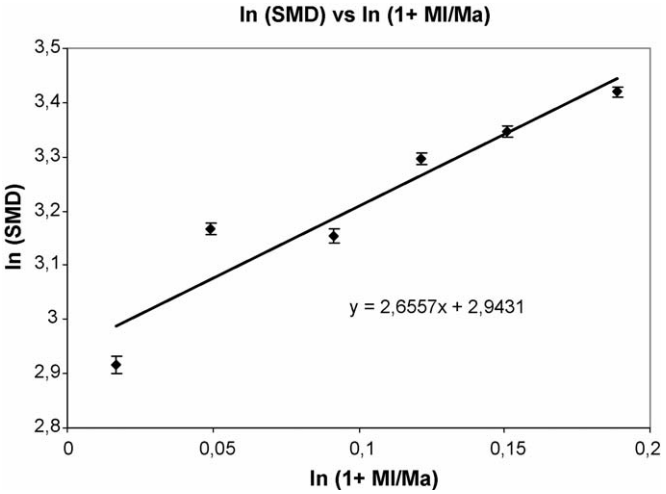

Fig. 5. Dependence between SMD and $(1 + (\dot{M}_l/\dot{M}_a))$.

The linear dependence between SMD and $(1 + (\dot{M}_l/\dot{M}_a))$ is based on momentum balance and energy considerations:

$$\dot{M}_l U_l + \dot{M}_a U_a = (\dot{M}_l + \dot{M}_a) V_d \tag{11}$$

where V_d is the velocity of the atomized drop and the atomizing air after transferring part of its kinetic energy to the liquid. It is assumed that the total surface energy of the atomized droplets is proportional to the loss of kinetic energy:

$$\sum N_i d_i^2 \sigma_S = f[(\dot{M}_l U_l^2 + \dot{M}_a U_a^2) - (\dot{M}_l + \dot{M}_a) V_d^2] \tag{12}$$

where N_i is the number of droplets with diameters d_i produced per unit time and σ_S is the droplet surface energy per unit area. Substituting Eq. (11) and

$$\dot{M}_l = \pi \rho_l \sum \frac{N_i d_i^3}{8} \tag{13}$$

into Eq. (12) yields

$$\text{SMD} = f\left[1 + \left(\frac{\dot{M}_l}{\dot{M}_a}\right)\right] \tag{14}$$

where

$$\text{SMD} = \frac{\int_0^\infty D^3 \, dN}{\int_0^\infty D^2 \, dN} \tag{15}$$

3.3. Dependence of SMD on the Weber number

Experiments were conducted to examine the influence of the Weber number on the SMD. The effect of Weber number on the microcapsule SMD was examined by varying the air exit velocity. No variations of surface tension were undertaken. The data presented in Fig. 6 (SMD versus Weber number) were used to establish the functional dependence of the SMD on the Weber number. Fig. 6 shows that the SMD decreases with increasing Weber number.

The power dependence on the Weber number is examined by plotting the SMD data as a function of the Weber number at constant $(1 + (\dot{M}_l/\dot{M}_a))^{2.66}$. It has been previously established

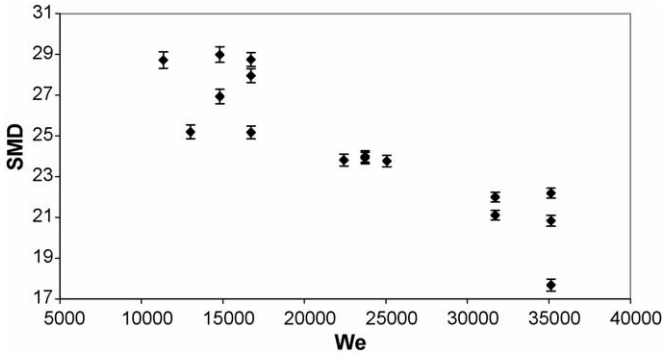

Fig. 6. Variations of SMD with Weber number.

that the effects of the air flow on the viscous behaviour of the polymeric solutions are negligible. Recall that the power dependence X_Z of the SMD was nearly constant, irrespective of the Weber number [29]. In Section 3.2 it was also established that the power dependence of SMD on $(1 + (\dot{M}_l/\dot{M}_a))$ was 2.66. Thus, in order to extract the Weber number power dependence from the data presented in Fig. 6 should be correlated according to the following relation:

$$\frac{\text{SMD}}{(1 + (\dot{M}_l/\dot{M}_a))^{2.66}} = f(We)^{X_{We}} \tag{16}$$

A logarithmic representation of SMD of the microparticles versus the logarithm of the Weber number at constant $(1 + (\dot{M}_l/\dot{M}_a))^{2.66}$ (Fig. 7) show that the power dependence between the SMD and the Weber number is given by the following relation:

$$\frac{\text{SMD}}{(1 + (\dot{M}_l/\dot{M}_a))^{2.66}} = f(We)^{-0.2718} \tag{17}$$

3.4. Semi-empirical model for air-blast atomization

Based on the above-mentioned wave mechanism, and considering the models proposed by Mansour and Chigier [29] for atomization of non-Newtonian fluids, the following two- and three-parameter equations are proposed to predict the particle

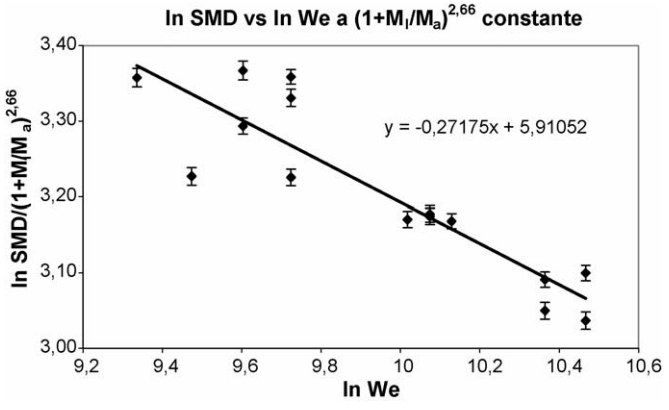

Fig. 7. Influence of the Weber number on the Sauter mean diameter of the microcapsules.

Table 2
Unknown variables for Eqs. (18) and (19)

	X_1	X_2	X_3
Eq. (18)	0.2717 ± 0.0214	0.2771 ± 0.0214	−8.1992E−03 ± 1.827E−03
Eq. (19)	0.2717 ± 0.0214	0.2996 ± 0.0214	–

size of the microcapsules obtained:

$$\frac{\text{SMD}}{D} = \left(1 + \frac{\dot{M}_l}{\dot{M}_a}\right)^{2.66} [X_2 We^{-X_1} + X_3 Z^{X_1}] \tag{18}$$

$$\frac{\text{SMD}}{D} = \left(1 + \frac{\dot{M}_l}{\dot{M}_a}\right)^{2.66} \left[X_2 \left(\frac{Z}{We}\right)^{X_1}\right] \tag{19}$$

where D is the discharge orifice diameter.

According to Eqs. (18) and (19) together with the experimental data of microcapsules sizes the unknown variables, X_1, X_2, X_3 were obtained (Table 2).

3.4.1. Comparison between experimental microcapsules size and model predictions

In order to obtain the experimental variation of the SMD of the microcapsules (behaviour curves) the effect of sodium alginate flow rate and the air flow rate were studied. The experimental microcapsules sizes obtained were compared with the models predicted sizes.

3.4.1.1. Sodium alginate flow rate variation. The first set of experiments were carried out at constant value of pressurized flow air of 138 l/min and the sodium alginate flow rate was modified ranged from 0.003 to 0.037 l/min. It was previously checked, that sodium alginate flow rates lower than 0.003 l/min, did not generate an homogeneous regimen and flow rates higher than 0.037 l/min produced agglomerates.

The experimental SMD data obtained from the different experiments and the theoretical size of the microcapsules, calcu-

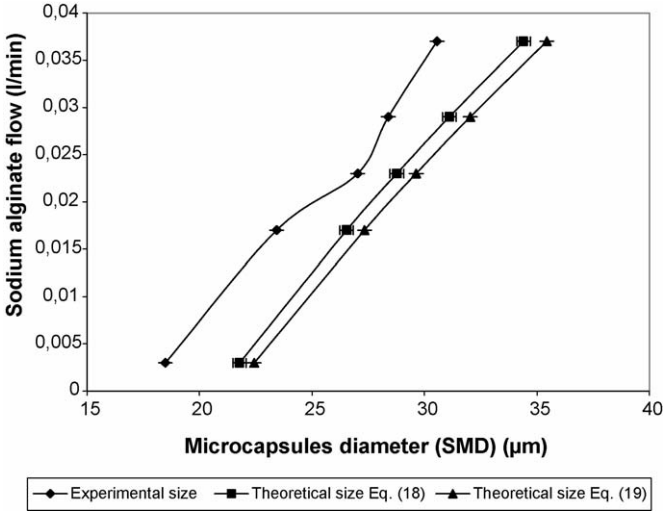

Fig. 8. Calculated by Eqs. (18) and (19) vs. SMD measured.

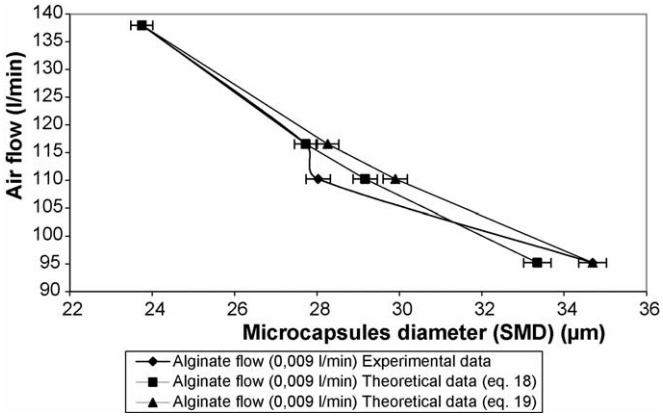

Fig. 9. Agreement between the experimental data and the theoretical data (variation of the air flow at a constant alginate flow, 0.009 l/min).

lated from Eqs. (18) and (19) are collected and were represented in Fig. 8. From this figure it can be seen that there is a very good agreement between the experimental data obtained and both proposed models.

3.4.1.2. Pressurized air flow rate variation. The second set of experiments was carried out at different pressurized air flow rate ranged from 78.40 to 138.00 l/min, at different constant flows of sodium alginate (0.003, 0.006, 0.009 l/min). Flow rates of pressurized air lower than 78.40 l/min, did not generate atomization. However, flow rates higher than 138.00 l/min generated turbulences on the of the barium chloride solution surface when atomization is performed.

The experimental SMD data obtained from the different experiments and the theoretical size of the microcapsules, calculated from Eqs. (18) and (19) are collected and were represented in Figs. 9–11. From this figures it can be seen that there is a very good agreement between the experimental data obtained and both proposed models.

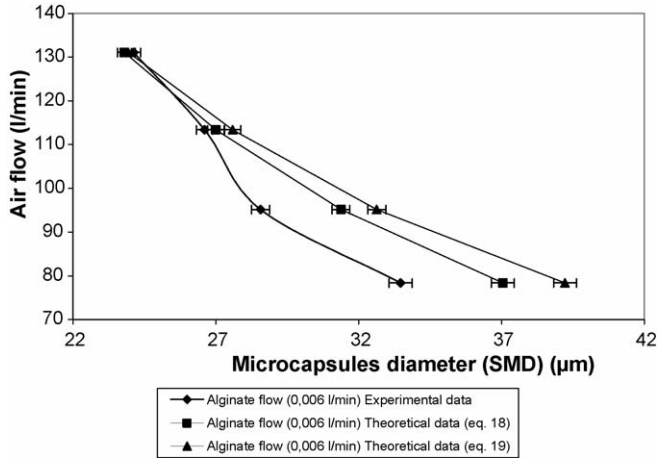

Fig. 10. Agreement between the experimental data and the theoretical data (variation of the air flow at a constant alginate flow, 0.006 l/min).

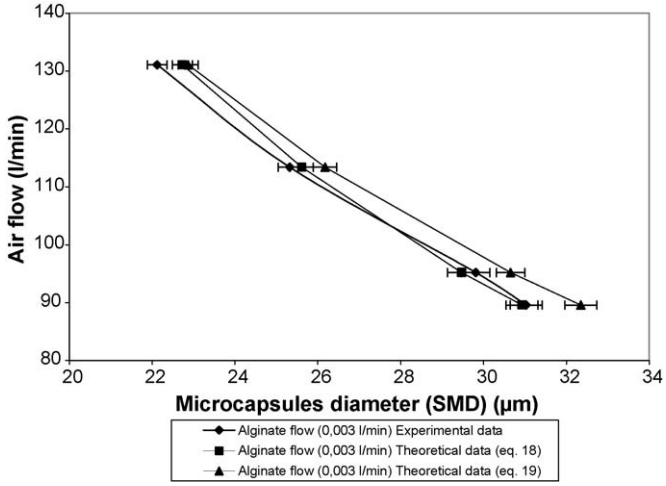

Fig. 11. Agreement between the experimental data and the theoretical data (variation of the air flow at a constant alginate flow, 0.003 l/min).

4. Conclusions

It is the first time that two semi-empirical models have been proposed to predict the particle size obtained from a microencapsulation technology of polyelectrolyte complex beads, which produce based in atomization processes. The polymer used was sodium alginate as polyanion and barium chloride solution as polycation. To do that, an air-blast atomizer, was used.

The accuracy of the wave-mechanisms-based models in predicting droplet size after breakup of alginate solution has also been demonstrated. The atomized microparticle size were expressed in terms of three dimensionless groups, the liquid/air mass ratio, the Weber number and the Ohnesorge number in simple forms whose exponents and coefficients were determined by least-squares fit to the experimental data. The best correlations were found for the equations involving the exponent of the *Z*-dependency equal to the exponent of the *We*-dependency. This verifies the basic hypothesis that at the conditions of this study the waves propagate as acceleration waves.

There is a good agreement between the data obtained from the proposed models and the experimental data. This shown that the air-blast atomization theory can be used to predict the particle size obtained in a microencapsulation technique based in atomization processes.

References

[1] D.J. Burgess, J.E. Carless, Manufacture of gelatine/gelatine coacervate microcapsules, Int. J. Pharm. 27 (1987) 61–70.
[2] S. Benita, J.P. Benoit, F. Puisieux, C. Thies, Characterization of drug-loaded poly (D,L-lactide) microspheres, J. Pharmacol. Sci. 73 (1984) 1721–1724.
[3] T. Sato, M. Kanke, H. Schroeder, P. DeLuca, Porous biodegradable microspheres for controlled drug delivery. I. Assessment of processing conditions and solvent removal techniques, Pharm. Res. 5 (1988) 21–30.
[4] D.J. Burgess, S.S. Davis, E. Tomlinson, Potential use of albumin microspheres as a drug delivery system. I. Preparation and in vitro release of steroids, Int. J. Pharm. 39 (1987) 129–136.
[5] F.-L. Mi, T.-B. Wong, S.-S. Shyu, S.-F. Chang, Chitosan microspheres: modification of polymeric chem-physical properties of spray-

dried microspheres to control the release of antibiotic drug, J. Appl. Polym. Sci. 71 (1999) 747–759.
[6] L. Bilancetti, M. Bucko, B. Bugarski, J. Bukowski, P. Gemeiner, D. Lewinska, V. Manojlovic, B. Massart, C. Nastruzzi, V. Nedovic, D. Poncelet, U. Pruesse, S. Rosinski, S. Siebenhaar, L. Tobler, A. Vikartovska, K. Vorlop, Round robin experiment "Bead production technologies", University of Perugia, Faculty of Pharmacy, Department of Chemistry and Pharmaceutical Technology of Drugs.
[7] Y. Senuma, C. Lowe, Y. Zweifel, J.G. Hilborn, I. Marison, Alginate hydrogel microspheres and microcapsules prepared by spinning disk atomization, Biotechnol. Bioeng. 67 (2000) 616–622.
[8] Y. Senuma, J.G. Hilborn, Key parameters for monodispersed polymer microspheres with spinning disk atomization, Mater. Res. Innov. 3 (1999) 42–49.
[9] D. Serp, E. Cantana, C. Heinzen, U. von Stockar, I.W. Marison, Characterization of an encapsulation device for the production of monodisperse alginate beads for cell immobilization, Biotechnol. Bioeng. 70 (2000) 41–53.
[10] C. Shwinger, A. Klemenz, K. Busse, J. Kressler, Encapsulation of living cells with polymeric systems, Macromol. Symp. 210 (2004) 493–499.
[11] L. Canaple, A. Rehor, D. Hunkeler, Improving cell encapsulation through size control, J. Biomater. Sci. Polym. Ed. 13 (2002) 783–796.
[12] R. Robitaille, J.F. Pariseau, F.A. Leblond, M. Lamoureux, Y. Lepage, J.P. Hallé, Studies on small (<350 μm) alginate-poly-L-lysine microcapsules. III. Biocompatibility of smaller versus standard microcapsules, J. Biomed. Mater. Res. 44 (1999) 116–120.
[13] G. Orive, R.M. Hernandez, A.R. Gascón, M. Igartua, J.L. Pedraz, Development and optimization of alginate–PMCG–alginate microcapsules for cell immobilization, Int. J. Pharm. 259 (2003) 57–68.
[14] S. Sugiura, T. Oda, Y. Izumida, Y. Aoyagi, M. Satake, A. Ochiai, N. Ohkohchi, M. Nakajima, Size control of calcium alginate beads containing living cells using micro-nozzle array, Biomaterials 26 (2005) 3327–3331.
[15] A.H. Lefebvre, Atomization and Sprays, Hemisphere, New York, 1989.
[16] E. Giffen, A. Muraszew, The Atomization of Liquid Fuels, John Wiley, New York, 1953.
[17] N. Chigier, Energy Combustion and the Environment, McGraw-Hill, New York, 1981.
[18] R.L. Panton, Incompressible Flow, John Wiley and Sons Inc., 1995.
[19] N. Dombrowski, W.R. Johns, The aerodynamic instability and disintegration of viscous liquid sheets, Chem. Eng. Sci. 18 (1963) 203–214.
[20] J. Shen, X. Li, Instability of an annular viscous liquid jet, Acta Mech. 114 (1996) 167–183.
[21] J. Shen, X. Li, Breakup of annular viscous liquid jets in two gas streams, AIAA J. 12 (1996) 752–759.
[22] W.T. Kim, S.K. Mitra, S. Li, L.A. Prociw, T.C.J. Hu, A predictive model for the initial droplet size and velocity distributions in sprays and comparison with experiments, Part. Part. Syst. Char. 20 (2003) 135–149.
[23] M. Adelberg, Breakup rate and penetration of a liquid jet in a gas stream, AIAA J. 5 (1967) 1408–1415.
[24] M. Adelberg, Mean drop size resulting from the injection of a liquid jet into a high-speed gas stream, AIAA J. 6 (1968) 1143–1147.
[25] H. Jeffreys, On the formation of water waves by wind, Proc. Roy. Soc. Lond. A 107 (1925) 189.
[26] E. Mayer, ARS J. 31 (1961) 1783–1785.
[27] N.K. Rizt, A.H. Lefebvre, Influence of liquid film thickness on air-blast atomization, J. Eng. Power Trans. ASME 102 (1980) 706–710.
[28] T. Arai, H. Hashimoto, Disintegration of a thin liquid sheet in a cocurrent gas stream, in: Proceedings of the 3rd International Conference of Liquid Atomization and Spray Systems, 1985, V1B/1/1-8.
[29] A. Mansour, N. Chigier, Air-blast atomization of non-Newtonian liquids, J. Non-Newton. Fluid Mech. 58 (1995) 161–194.